Radiation of Logarithmic Spiral Antennas in the Presence of Dense Dielectric Lenses

Garufo, Alessandro; Llombart Juan, Nuria; Neto, Andrea

DOI
10.1109/TAP.2016.2593744

Publication date
2016

Document Version
Accepted author manuscript

Published in
IEEE Transactions on Antennas and Propagation

Radiation of Logarithmic Spiral Antennas in the Presence of Dense Dielectric Lenses

Alessandro Garufo, *Student Member, IEEE*, Nuria Llombart, *Senior Member, IEEE*, and Andrea Neto, *Fellow, IEEE*

***Abstract*— In this paper, the performance of logarithmic spiral antennas as feeds of dense dielectric lens are investigated in detail. The performances are evaluated in terms of clean symmetric radiation patterns, high polarization purity, antenna efficiency, and radiation dispersivity. A logarithmic spiral antenna placed in the dielectric-air interface can provide high aperture efficiencies over large bandwidths if coupled to a synthesized elliptical lens. The use of an air gap increases the directivity of the spiral radiation inside the dielectric allowing for lens directive patterns without sidelobes and reducing the dispersivity of the radiated pulse. The directivity enhancement of the fields inside the dielectric is validated by the measurement of a prototype. The highest frequency at which these antennas can be fed by a planar microstrip line is limited by the thickness of the microstrip substrate.**

***Index Terms*— Dispersion, leaky-wave antenna, lens antenna, spiral antenna, ultrawideband antenna.**

I. Introduction

DIELECTRIC lenses fed by planar antennas have been proposed for many applications in the millimeter-wave (mm-wave) and sub-mm-wave systems [1]–[11]. In particular, planar frequency independent antennas are used as lens feeds to achieve wideband operation [5]–[11], since they operating bandwidth (BW) is mainly limited by their size [12]. More specifically, it has been pointed out that the self-complementary structures in free space ensure a constant impedance behavior [13].

In the presence of a dielectric lens, self-complementary antennas preserve their constant impedance behavior, but their radiation is different from the one in free space. Indeed, they not longer act as self-complementary structures [14]. The difference is the additional leaky wave mechanism that characterizes the radiation of a planar antenna at the interfaces between air and dielectric [15], [16]. Therefore, the geometries optimized for free-space radiation [17]–[22] cannot be directly scaled in order to be used as lens feeds. In this paper, we focus on analyzing the radiation properties of logarithmic spiral in the presence of dielectric lenses. The designs are tuned to achieve an operative BW of a decade when fed by an integrated feed. We also show the sharp degradation of the performances that effects such kind of antennas, when an embedded planar transmission line is used as feeding system, e.g., microstrip or coplanar waveguide.

Manuscript received September 23, 2015; revised June 27, 2016; accepted July 12, 2016. Date of publication July 21, 2016; date of current version October 4, 2016. This work was supported by European Research Council Starting Grants ERC-2011-StG Grant AAATSI no. 278794.

The authors are with the Microelectronics Department of the Electrical Engineering, Mathemathics and Computer Science Faculty, Delft University of Technology, Delft 2628 CD, The Netherlands (e-mail: a.garufo@tudelft.nl; n.llombartjuan@tudelft.nl; a.neto@tudelft.nl).

Color versions of one or more of the figures in this paper are available online at http://ieeexplore.ieee.org.

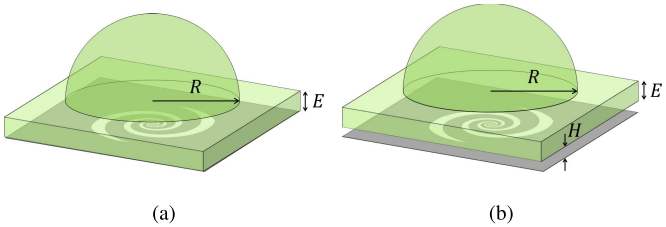

(a) (b)

Fig. 1. Lens antennas. (a) Spiral antenna with an elliptical lens for incoherent imaging system. (b) Enhanced spiral antenna with an hyperhemispherical lens for coherent imaging system.

There have been several works optimizing the dispersivity of spiral geometries in free space [21], [22]. When a spiral antenna is used as a dense dielectric lens feed, its dispersivity will be affected. In this paper, we show that by introducing a small gap between the spiral and the dielectric in the presence of an hyperhemispherical lens, see Fig. 1(b), the frequency dispersion of the spiral is not altered by the lens anymore. Indeed the dispersivity generated by the lens antenna is practically the same as the one introduced by the spiral geometry. The use of a small gap has been previously proposed in the presence of slot antennas leading to broadband nondispersive operation [23], [24].

This paper is organized as follows. In Section II, the analysis of the spiral antenna when radiating between two half-infinite dielectric media is discussed. In this case, the self-complementary structure does not provide the best performances because of the presence of the leaky wave phenomena. We also shown that the introduction of a small gap enhances the directivity of the fields radiated into the dense medium. In Section III, the impact of planar feeding system on the performances of the antenna is discussed. Measurements from a prototype demonstrator of the enhanced spiral antenna feed are shown in Section IV, in order to prove the enhancement effect due to the presence of the air cavity between the bottom dielectric–air interface of the lens and the antenna. In Section V, the two proposed spirals are then coupled to a dielectric lens, the radiation performance and the dispersion of the pulse radiated by the lens fed by the two spiral feeds are shown and compared.

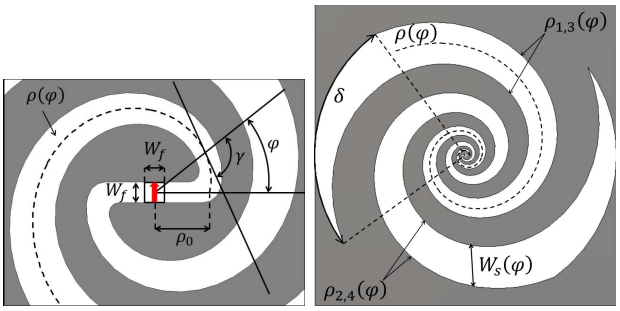

(a) (b)

Fig. 2. Logarithmic spiral antenna. (a) Antenna geometry. (b) Design parameters.

II. Logarithmic Spiral Antenna in Between Infinite Dielectrics

Spiral antennas radiating intro free space can achieve high quality omnidirectional patterns over large BWs [17]–[22]. However, the radiated power is divided equally into the upper and lower spaces. In order to improve the directionality of these antennas, one can resort to the use of a ground plane that limits the operational BW, or alternatively a dense dielectric that renders the system almost unidirectional. When a spiral antenna is placed at the air–dielectric interface, the structure is not more self-complementary [14]. The standard free space geometries cannot be simply scaled to match two different dielectric constants.

In order to design a two arms spiral antenna, each of the arms of the spiral has to be defined by means of two curves which represent the edges of each arm [17] as in Fig. 2(b). Three parameters are needed: the starting radius ρ_0, the curvature angle γ, and the winding number N

$$\text{Arm 1:} \quad \rho_{1,3}(\varphi) = \rho_0 e^{a\left(\varphi_1 \pm \frac{\delta}{2}\right)} \tag{1a}$$

$$\text{Arm 2:} \quad \rho_{2,4}(\varphi) = \rho_0 e^{a\left(\varphi_2 \pm \frac{\delta}{2} + \pi\right)} \tag{1b}$$

where $\varphi_1 \in [0, 2\pi N]$ and $\varphi_2 \in [-\pi, 2\pi(N - (1/2))]$ and $a = 1/\gamma$; the two arms are identical and rotated of π one respect to each other; the parameter δ is the rotational angle between the two edges of each arm and it determines the tapering factor of the spiral arms. The length of the spiral arms in function of the rotational angle can be easily evaluated integrating the differential path along the spiral curve derived by equation of the locus of the spiral [17].

This section is dedicated to the analysis of the spiral placed at the interface between free space and an infinite dielectric half space. The dielectric half space simulates, to the first order, the effect of a dielectric lens on the planar antenna. The spiral geometry is aimed at achieving rotationally symmetric patterns with high circular polarization purity over a decade BW from 5 to 50 GHz. Different logarithmic spirals have been simulated using CST simulations [27], radiating in an infinite dielectric medium with absorbing boundaries at the edge of the dielectric.

A. Spiral Radiation Between Two Homogenous Media

Initially, the antenna is assumed to be printed at the interface between air and silicon, $\epsilon_{r1} = 1$ and $\epsilon_{r2} = 11.9$, respectively.

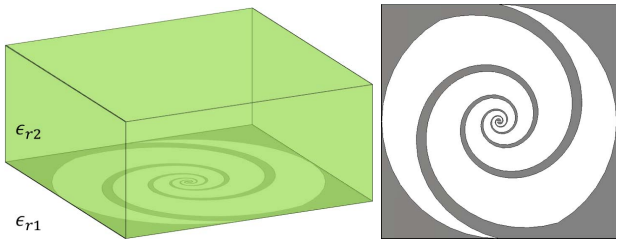

(a) (b)

Fig. 3. Logarithmic spiral antenna between two homogeneous medium. (a) Regular structure and (b) geometry of the spiral for the regular structure ($\rho_0 = 0.177$ mm, $\delta = 150°$, $\gamma = 76.5°$, $N = 2.6$, and $W_f = 0.059$ mm).

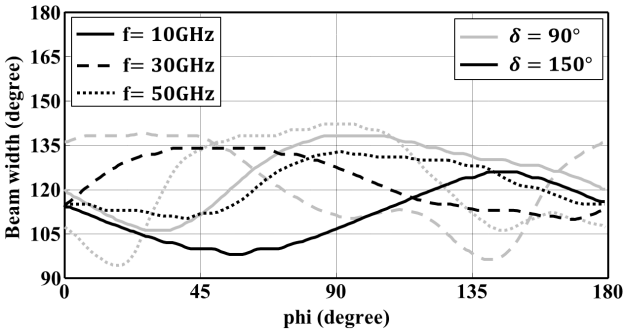

Fig. 4. Width of the beams at -10 dB inside the dielectric of the regular structure for the self-complementary ($\delta = 90°$) and optimized structure ($\delta = 150°$).

When the spiral antenna is fed at its center as in Fig. 2(a), the characterizing (magnetic) current propagates along the arms at the interface between the two dielectric with a phase constant which is the roughly the average of the phase constants of the two medium

$$\beta \approx \sqrt{\frac{\epsilon_{r1} + \epsilon_{r2}}{2}} k_0 = \epsilon_{\text{eff}} k_0 \tag{2}$$

where k_0 is the propagation constant in free space. Typically, in the literature [8], [9], ϵ_{eff} is used as scaling factor in order to scale the antenna geometries from the free space design to the half space design. While this approach is adequate for the basic dimensioning of the spiral (i.e., the maximum and minimum operating frequencies), the quality of the patterns obtained resorting only to this scaling is not optimal. In fact, the effective propagation constant β results in a fast wave for the denser medium and a slow wave for the free space. Thus, the radiation mechanism, occurring to the currents flowing at the interface between two different media, is heavily affected by the distributed leaky-wave radiation [15], [16]. In order to account for this effect, the tapering angle δ had to be varied to achieve the best possible quality of the radiation patterns inside the dielectric. The geometry of the best structure, we could come up with ($\gamma = 76.5°$ and $\delta = 150°$), is shown in Fig. 3(b), which is significantly different that the self-complementary ($\delta = 90°$) in Fig. 2(b). Because of the increasing of the tapering angle of the slot arms, the ground plane between the arms is significantly reduced. In this case, the structure can be referred to as dipole spiral rather than as slotted spiral. In Fig. 4 are shown the widths of the beam at -10 dB for $\delta = 90°$ and for the geometry $\delta = 150°$. The self-complementary inspired geometry ($\delta = 90°$) does not provide

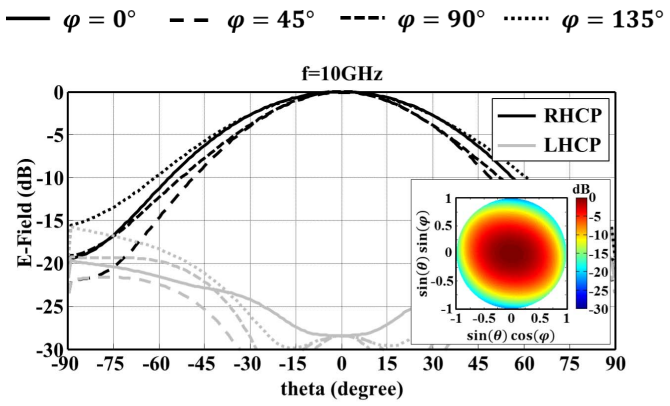

(a)

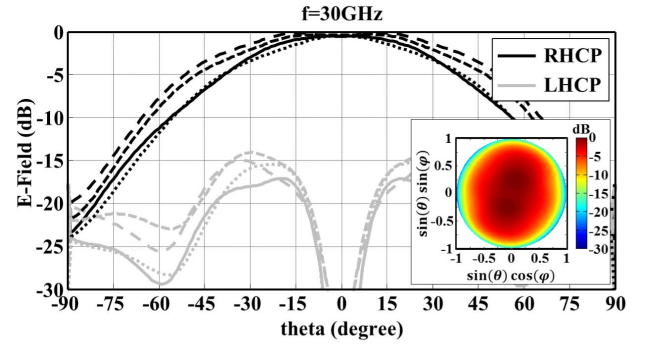

(b)

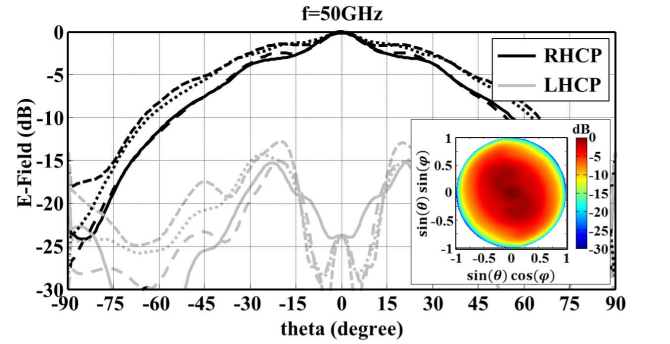

(c)

Fig. 5. Simulated radiation patterns (primary fields) of the logarithmic spiral antenna ($\delta = 150°$) inside the dielectric on different φ planes at the frequencies (a) 10GHz, (b) 30GHz and (c) 50GHz. Insets: 2-D radiation patterns of the RHCP component.

the best symmetric pattern for spirals printed between two dielectrics. Because of the curvature angle is the same for both the structures, they present the same average width of the beams, but increasing the tapering of the arms the spiral radiates less elliptical patterns with an average variation of the width of 40° for $\delta = 90°$ to 24° for $\delta = 150°$. For the $\delta = 150°$ geometry, the Wobble of Wave (ratio between the maximum and the minimum of the field magnitude at constant elevation angle θ_0 [25]) at $\theta = 30°$ is 1.71, 2.14, and 1.8 dB, respectively, for 10, 30, and 50 GHz.

The normalized radiation patterns inside the dielectric are shown in Fig. 5. The radiated patterns are plotted as a right-handed circular polarization (RHCP) and the left-handed

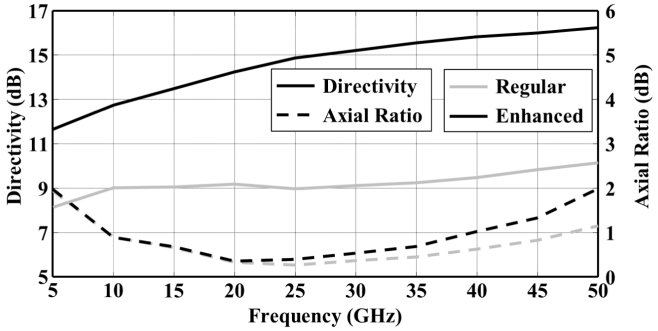

Fig. 6. Simulated broadside directivity and axial ratio inside the dielectric of the regular and the enhanced structures.

TABLE I

PROPOSED ANTENNAS VERSUS STATE-OF-THE-ART ANTENNAS AVERAGE BEAMWIDTHS OF THE PRIMARY FIELDS

	Beam width			
	5GHz	20GHz	35GHz	50GHz
Proposed Regular spiral	146°	122°	124°	121°
Enhanced spiral	96°	70°	57°	48°
	Beam width			
	6GHz	12GHz	18GHz	24GHz
Sinuous antenna in [8]	129°	130°	133°	125°
	Beam width			
	2.5THz		4.3THz	
Spiral antenna in [9]	125°		120°	

circular polarization (LHCP). The circular polarization is calculated combining two linear polarization according to Ludwig's third definition [28]. The beams of the RHCP component show constant widths around 122° and the LHCP component is below -13 dB over the entire BW. The antenna provides a constant directivity over the entire decade BW as shown in Fig. 6. The reflection coefficient is below -10 dB for a reference impedance of 50 Ω.

For sake of comparison, the proposed logarithmic spiral ($\gamma = 76.5°$ and $\delta = 150°$) is compared with other frequency independent antennas available in the literature [8], [9]. Even if they are operating at different frequencies, the three structures have been designed for exciting a dense dielectric lens. It is worth noting that all the proposed frequency independent antennas have roughly the same directivity. However, the proposed spiral presents the most symmetric patterns. Table I presents a detailed comparison of the simulated beamwidths at widely spaced frequency points.

B. Enhanced Radiation

It is possible to increase the directivity of the patterns radiated by an antenna into a dense dielectric by introducing an electrically small air gap [23]. This implies that the spiral antenna should be printed on a small membrane at distance H from the lens itself. This structure will be indicated as the enhanced structure and it is shown in Fig. 7(a). The introduction of an air cavity between the dielectric interface and the antenna feed has been already proposed as solution to improve the illumination efficiency of linear polarized lens antenna feeds [23], [24], [26]. The presence of the small air gap, typically $H \leq \lambda_0/10$ with λ_0 at the highest frequency of operation, modifies the behavior of the leaky wave propagation

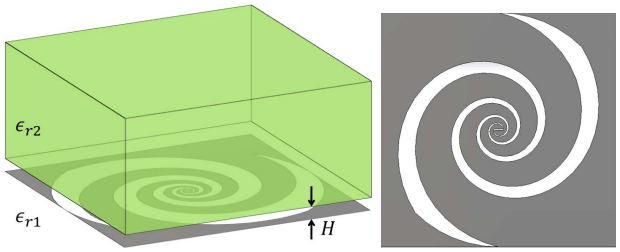

(a) (b)

Fig. 7. Logarithmic spiral antenna between two homogeneous medium. (a) Enhanced structure with the introduction of an air gap. (b) Geometry of the spiral for the enhanced structure ($\rho_0 = 0.6$ mm, $\delta = 45°$, $\gamma = 76.5°$, $N = 2.6$, and $W_f = 0.15$ mm). The height of the air cavity is $H = 0.4$ mm.

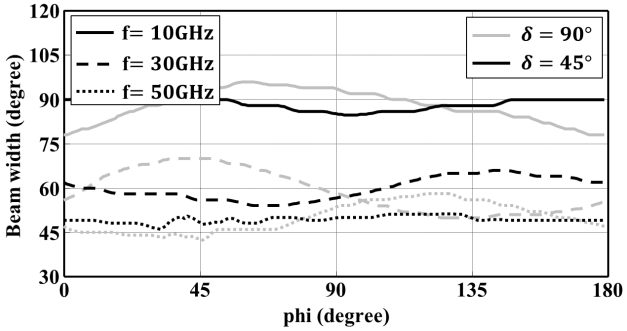

Fig. 8. Width of the beams at -10 dB inside the dielectric of the enhanced structure for the self-complementary ($\delta = 90°$) and optimized structure ($\delta = 45°$).

which tends to the value in free space $\beta \approx k_0$. Moreover, the enhanced structure supports an additional leaky mode localized in the cavity, which propagates orthogonally to the radiating slot enhancing the rotational symmetry of the patterns [26].

Since the current propagates with the free space velocity, the dimensioning of the spiral is the same as that one in free space for the highest and lowest frequencies. The leaky wave distributed radiation can be controlled by appropriately tapering the spiral arms, setting the angles γ and δ, and the height H of the air cavity. This latter was set at $H = 0.4$ mm corresponding to $\lambda_0/15$ at the highest frequency. This ensures that the maximum loss due to front-to-back ratio over the entire BW from 5 to 50 GHz is lower than 1 dB.

The design includes a starting radius $\rho_0 = 0.6$ mm and the geometry of the optimum enhanced spiral is shown in Fig. 7(b). Even the designed enhanced structure ($\gamma = 76.5°$ and $\delta = 45°$) is significantly different from the self-complementary structure. The behavior of the beamwidth in function of the frequency is also controlled by the height of the air cavity which dictates the increase of the directivity as function of the frequency. The symmetry of the radiation patterns is controlled by both the tapering angle δ and the cavity height H, reducing the tapering of the arms the ellipticity of the beams decreases. Fig. 8 shows the beam widths at -10 dB of the enhanced structure with the tapering angle $\delta = 90°$ and the tapering angle $\delta = 45°$. The beams of the RHCP component are symmetric with a range of the variation, as a function of the azimuth angle, of the beam at -10 dB from 12°, for the lowest frequency, to 1° for the highest. The beamwidth

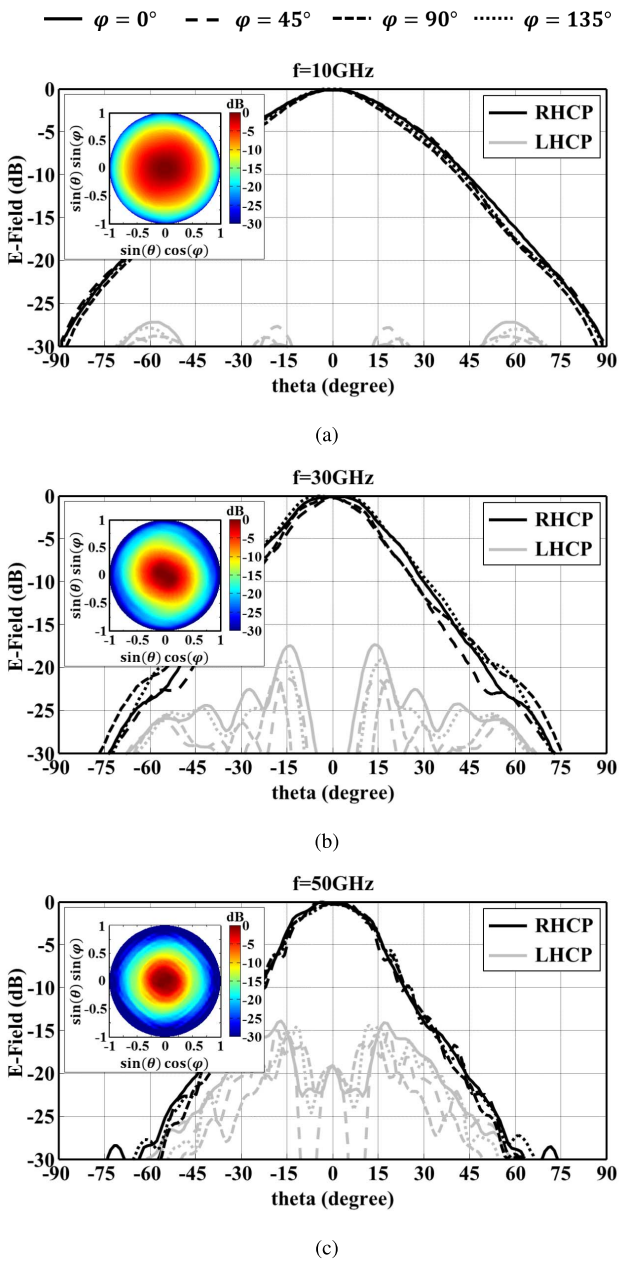

(a)

(b)

(c)

Fig. 9. Simulated radiation patterns (primary fields) of the enhanced logarithmic spiral antenna ($\delta = 45°$) inside the dielectric on different φ planes at the frequencies (a) 10GHz, (b) 30GHz and (c) 50GHz. Insets: 2-D radiation patterns of the RHCP component.

decreases in a range from 96° to 48° as the frequency increase. The normalized radiation patterns into the dielectric radiate by the proposed enhanced spiral antenna are shown in Fig. 9. The actual width of the beam also decreases as the frequency increases resulting in higher directivity as it shown in Fig. 6. The LHCP component of the field is below -13 dB over the entire frequency range. The reflection coefficient is below -14 dB for a reference impedance of 65 Ω.

III. Planar Feeding System

The performances of the spiral antennas, shown in Sections II-A and II-B, can be obtained only when the antenna transmitter/receiver is integrated at the center of the spiral. In order to send out/read a high frequency signal,

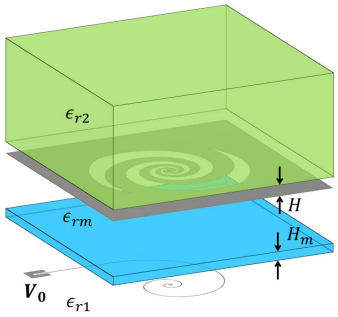

Fig. 10. Microstrip planar feeding system of the spiral antenna.

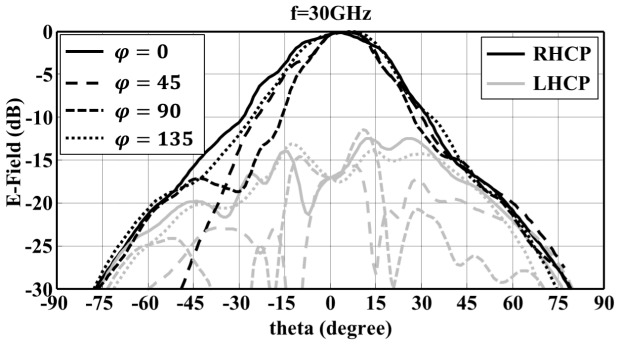

Fig. 11. Simulated radiation patterns of the enhanced logarithmic spiral antenna ($\delta = 45°$) fed by a microstrip on different φ planes at the frequency 30GHz.

the solutions proposed in the past were a coaxial cable embedded on the ground plane of the spiral [17], a differential feed using two coaxial cables orthogonally connected to the center of the antenna [21] or a microstrip [29], [30]. Only this last option is suited for mm-wave [31], [32], sub-mm-wave [33], [34] integrated systems. However, also microstrip feedings present challenges, in [29] and [30], it is indicated that the ratio between the width of the ground plane and the microstrip has to be at least 10 in order to avoid the influence of the transmission line on the performances of the spiral. According to such rule, for the enhanced spiral presented in Section II, the height of the substrate should be smaller than $\lambda_0/210$, at the highest frequency. For the case of the regular spiral printed on a dense dielectric, Section II-A, it is needed a substrate of $\lambda_0/2100$, since the smallest ground plane dimension in between the spiral arms is 10 times smaller than the enhanced spiral. This dimension is comparable to the one used in [31] and [32]. Moreover, the regular spiral presents a lower input impedance than the enhanced one, which involves to use a substrate even smaller in order to obtain the desired matching at the feeding point.

Despite the fact that these problems cannot be solved with current Printed Circuit Board (PCB) technology. A microstrip feed has been designed with the purpose to build a prototype. Only the enhanced spiral of Section II-B is considered due to the lower requirements on the microstrip substrate. The microstrip with a spiral profile is placed on a substrate attached at the bottom interface of the metallic plane where the slot spiral is etched as it shown in Fig. 10. The end of the microstrip is connected to the ground plane by a short-circuit pin. The smallest available thickness of the substrate (Rogers RT/Duroid 6002, $\epsilon_r = 2.94$) has been used $H_m = 0.127$ mm,

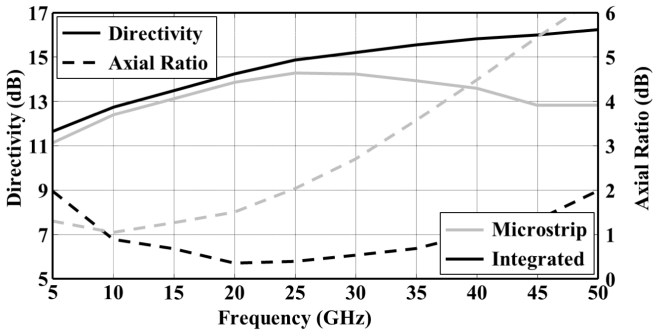

Fig. 12. Comparison of the simulated directivity and axial ratio at broadside direction between the enhanced spiral fed by the intgrated feed and microstrip.

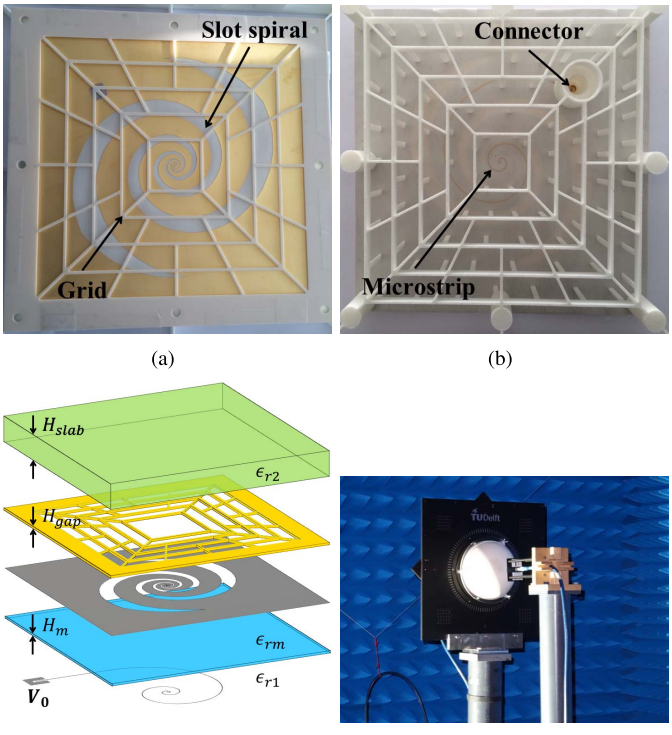

Fig. 13. Prototype of the enhanced spiral antenna and measurement setup. (a) Top view without the dielectric slab. (b) Bottom view. (c) Layered structure. (d) Measurement setup.

in order to design a matched microstrip with the smallest width possible $W_m = 0.2$ mm. Note that the height of the substrate and the microstrip width should have been smaller than $H_m = 0.028$ mm and $W_m = 0.044$ mm, respectively, to avoid the deterioration of the performance. Since the ratio between the ground plane, in the inner part of the spiral, and the width of such microstrip is smaller than the one indicates in [29] and [30], the microstrip feed introduces an imbalance in the structure. The micrsotrip itself radiates, resulting in tilted beams and asymmetric radiation patterns as is shown in Fig. 11. This effect is more relevant as the frequency increases because the radiation at higher frequencies occur in the inner part of the spiral where the ground plane is smaller, due to the tapered profile of the structure. Those effects are quantified in Fig. 12, the directivity at broadside is reduced and it starts decaying at the higher frequencies. Moreover the axial ratio is increased, affecting the circular polarization purity, resulting in a substantial reduction of the effective antenna BW.

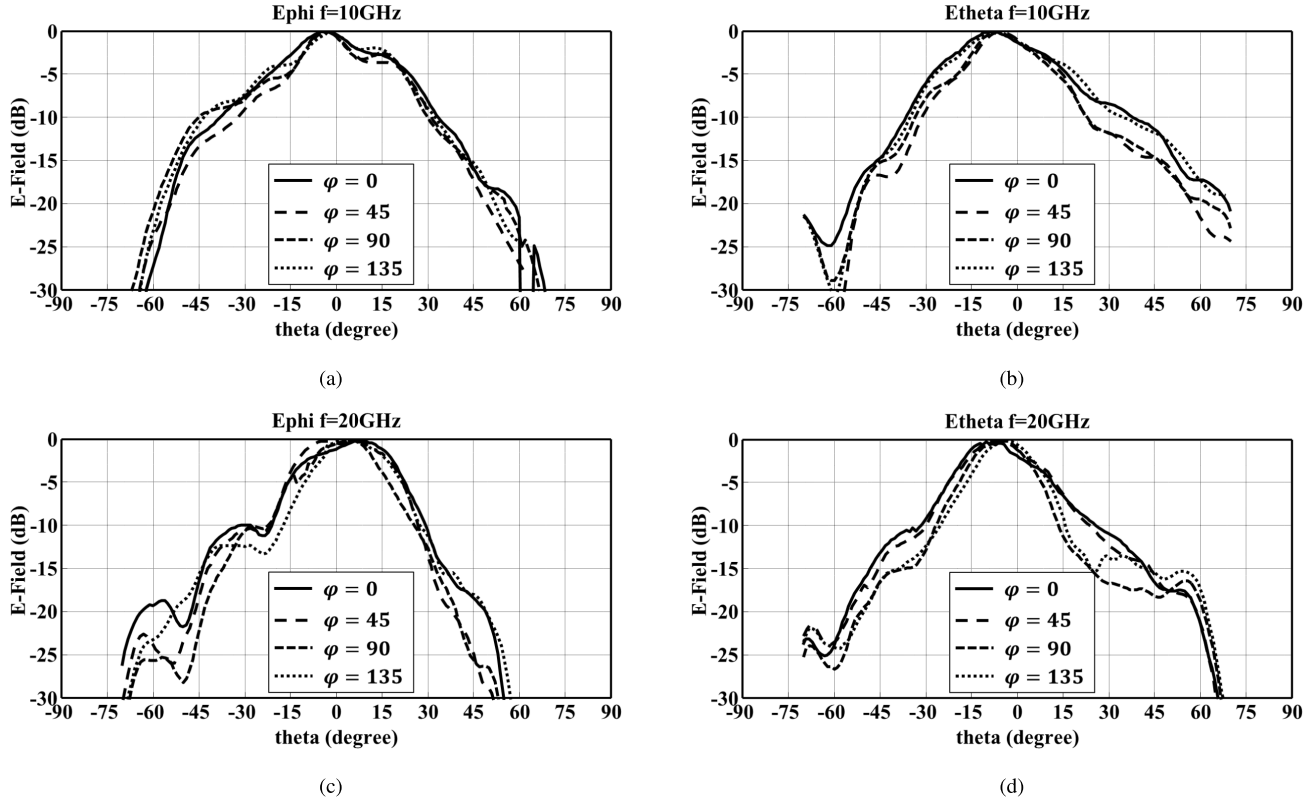

Fig. 14. Measured radiation patterns of the two spherical components inside the lens of the enhanced spiral prototype on different φ planes at the frequencies (a), (b) 10GHz and (c) (d) 20GHz; (a) (c) show the φ component, while (b), (d) show the θ component.

IV. Prototype Measurements

Despite the expectation of poor radiation performance due to the microstrip feeding, which can be improved when the antenna is realized with Integrated Circuit technology, typically used for high frequency applications [31], [32], a prototype demonstrator of the enhanced spiral has been manufactured in PCB technology. The main purpose of the prototype is to demonstrate the increase of the directivity, that can be achieved by introducing an air gap. The prototype combines the enhanced spiral antenna, a microstrip-based feeding and the use of an already available dielectric lens.

The prototype of the spiral is shown in Fig. 13(a) and (b), and the entire layered structure is shown in Fig. 13(c). The slot spiral is etched on the ground plane of a dielectric slab (Rogers RT/Duroid 6002, $\epsilon_r = 2.94$) of height $H_m = 0.127$ mm. The same dielectric slab is used as substrate for the microstrip line as is depicted in Fig. 13(c). The feeding line includes a transformer to match the line coupled with the spiral ($Z_0 = 70\ \Omega$) with the one that arrives to the connector ($Z_0 = 50\ \Omega$). The air gap is realized by a grid structure of height $H_{\text{gap}} = 0.4$ mm composed by a ceramic material (Rogers RT/Duroid 4003, $\epsilon_{rm} = 3.55$). The grid structure is designed to emulate the air cavity ($\epsilon_{\text{gap}} = 1$) and to ensure the mechanical stability of the structure. Lastly, to make the structure more stiff, the grid is attached to a thick slab of dielectric of height $H_{\text{slab}} = 3.2$ mm, which will be part of the extension length for the hemispherical lens. The material of the stiffening slab is the same which composes the lens (ECCOSTOCK HIK 500F, $\epsilon_{r2} = 11.9$). The realization of the air gap does not present any particular problem for microwaves and mm-wave applications and it can be easily realized using the procedure shown above. Difficulties arise at sub-mm-wave applications. Guaranteeing the designed thickness of the gap is critical and different dedicated process depending on the technological boundaries have to be adopted [35].

The spiral geometry of the prototype is slightly different respect to the structure presented in Section II-B. The starting radius has been enlarged in order to accommodate the microstrip, $\rho_0 = 0.75$ mm. The tapering angle has been increased from $\delta = 45°$ to $\delta = 58°$. The curvature angle is $\gamma = 76.5°$ and the number of windings is $N = 2.75$.

The measurements setup is shown in Fig. 13(d). In order to measure the patterns inside the lens, the spiral lens feed is placed at the bottom interface of the lens without the extension length and the probe is scanned along the lens surface. Eliminating the multiple reflections of the dielectric–air interface by means of time gating has been possible to evaluate the radiation patterns inside the lens as if the antenna is placed in a half semi-infinite dielectric. The broadband probe used for the measurements has a BW from 7 to 26 GHz.

The measured radiation patterns of the two linear polarizations are shown in Fig. 14 for different planes. The patterns are far less symmetric than one could have anticipated looking at the simulations from Section III. The reason is in the anisotropic behavior of the material of the dielectric lens [36]. To show the anisotropy, the radiation patterns in the $\varphi = 0°$ plane of the antenna has been measured for different rotation angles of the lens. The lens has been rotated four times with an angle step $\Delta\varphi = 30°$ and the measurements show significant changes with each rotation of the lens as it is shown

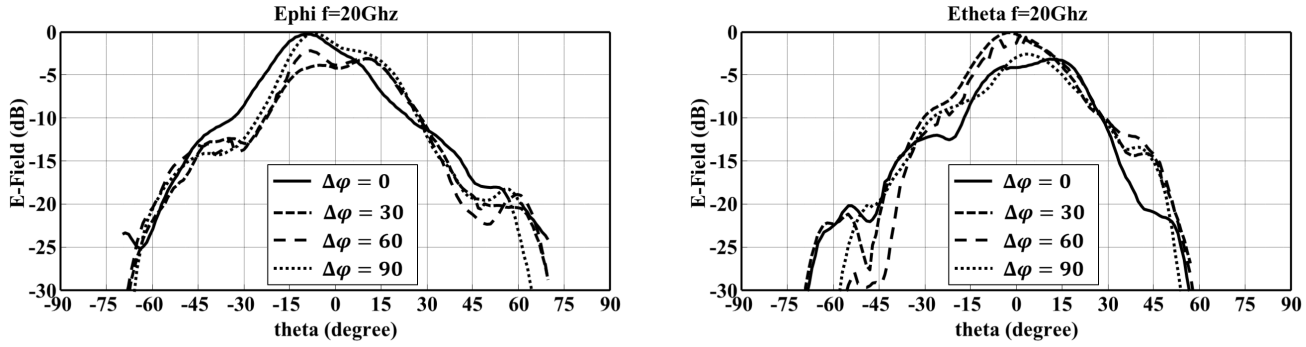

(a) (b)

Fig. 15. Measured radiation patterns inside the lens of the enhanced spiral prototype on the plane $\varphi = 0°$ at the frequency 20 GHz and at different rotation angles of the lens respect to the antenna feed; (a) shows the φ component, while (b) shows the θ component.

in Fig. 15. Because of this anisotropy, it is not possible to combine the linear polarizations in order to obtain the field in circular polarization inside the lens. Such undesired behavior of the dielectric lens can be avoided using silicon lenses [8], which have an isotropic behavior, and typically used in mm-wave and sub-mm-wave applications [5]–[7], [9], [31], [32]. Despite these problems, the patterns are still enlightening as they show beamwidths measured (taken as the value at -10 dB). The measured beamwidths vary from 75° to 55° against an expected beamwidths varying from 90° to 60°. The expected beamwidths of the regular spiral were in the order of 120°. This proves the dominance of the enhanced leaky wave mechanism, which is the main contribution of this paper.

V. Lens Radiation Performance

In this section, a comparison between the simulated performance of the regular and the enhanced spiral as feed of dense dielectric lenses are shown. The approach used for the characterization of the antenna is the same used in [26]. The simulated radiation patterns in an infinite dielectric, shown in Section II, are used to compute the fields radiated by the lens via a physical optics (PO) approach, [37], [38], without using any kind of correction of the PO currents by means of a transition function as proposed in [39], contributions associated with creeping waves [40] and the diffraction mechanisms induced by the lens truncation at the ground plane. In this approach the reflections at the lens interface is only included as a loss term in the gain and not in the evaluation of the shape of the lens radiation patterns. A silicon lens of diameter $D = 120$ mm, which corresponds to $20\lambda_0$ at 50 GHz, is chosen as a reference.

A. Radiation Patterns

The performance of a dense dielectric lens fed by the spiral antennas proposed in Section II are summarized in Fig. 16. The low frequency variation of the patterns of the regular spiral, Fig. 6, implies the possibility to achieve high aperture efficiency over a large BW by using a synthesized elliptical lens ($E = 0.39R$). The simulated gain for this case increases nearly quadratically with the frequency as expected. The aperture efficiency is between 45%–55% on the entire BW, only limited by the reflection losses, since no matching layers are assumed. Instead the gain of the synthesized elliptical lens fed by the enhanced spiral presents a lower frequency variation since a

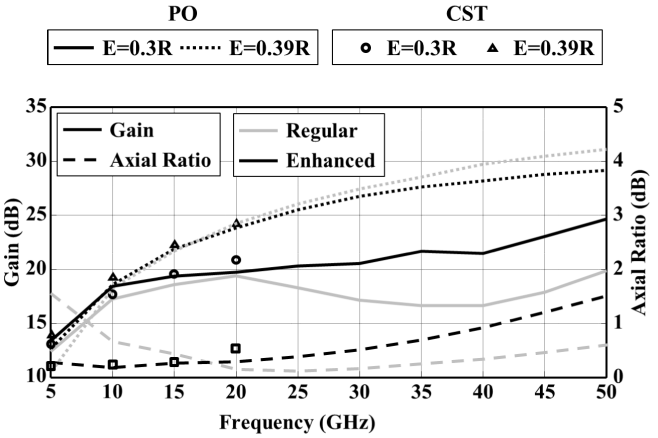

Fig. 16. Simulated broadside gain and axial ratio of the secondary fields for the regular and the enhanced structures using the hyperhemispherical and the elliptical extension. The gain takes into account of losses due to matching, reflection, polarization, and front-to-back ratio.

smaller portion of the lens is illuminated by the feed at high frequencies, but the patterns present nearly no sidelobes as shown in Fig. 17. The use of a regular spiral for low extension heights involves a significant decrease of the directivity at higher frequencies, due to the phase error on the currents at the lateral part of the lens [26]. Indeed, Fig. 16 shows such variation when the regular spiral is used with an extended hemispherical lens with $E = 0.3R$. Instead when the enhanced spiral is used as feed of such lens, Fig. 16 shows that the directivity increases linearly with the frequency. The use of an air gap allows to achieve clean radiated patterns for such low extension heights over the entire BW, as shown in Fig. 18, thanks to the enhanced directivity in the fields inside the dielectric.

In order to provide a further validation of the results shown in this section, a comparison of the performance of the enhanced spiral lens antenna evaluated by the PO approach and by CST simulations is provided. Both the hyperhemispherical and the elliptical extensions have been simulated using the time-domain solver of CST, without taking into account the effect of multiple reflections inside the lens. The simulations have been feasible only at the lower frequencies of the frequency band of interest, because of the heavy computational burden. A good agreement of the results between the PO method and the CST simulations has been observed as shown in Fig. 16. For sake of space only the comparison

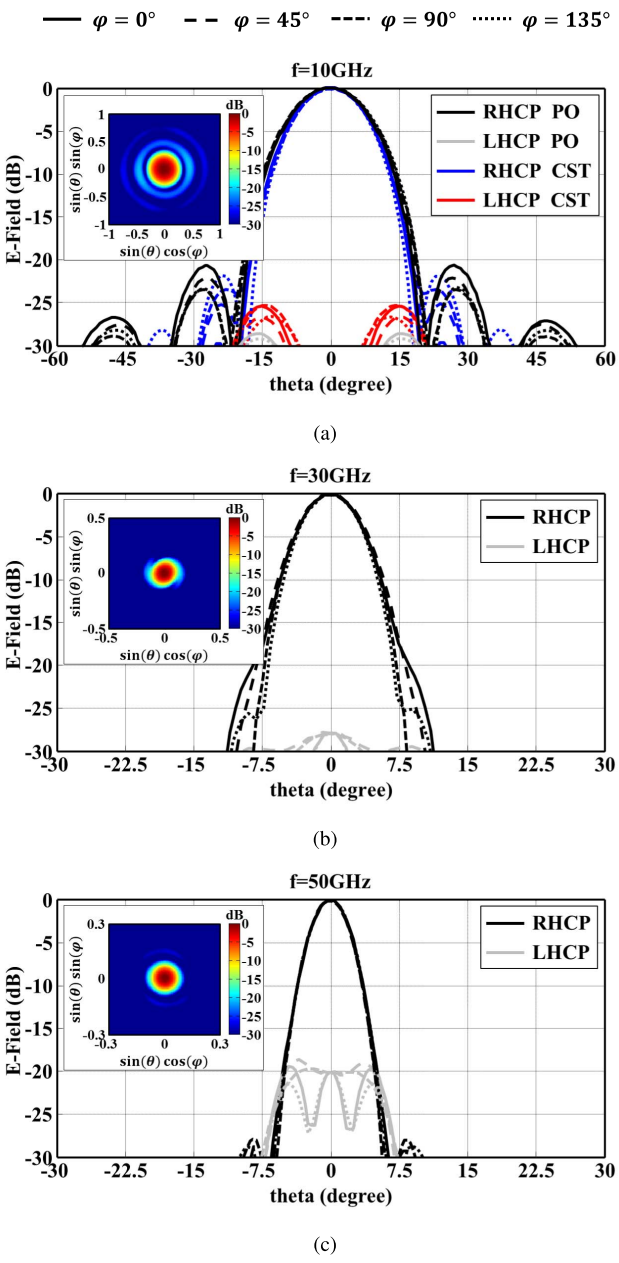

Fig. 17. Simulated radiation patterns outside the lens (secondary fields) illuminated by the enhanced spiral antenna feed at the elliptical point on different φ planes at the frequencies (a) 10GHz, (b) 30GHz and (c) 50GHz. Insets: 2-D radiation patterns of the RHCP component evaluated with the PO approach.

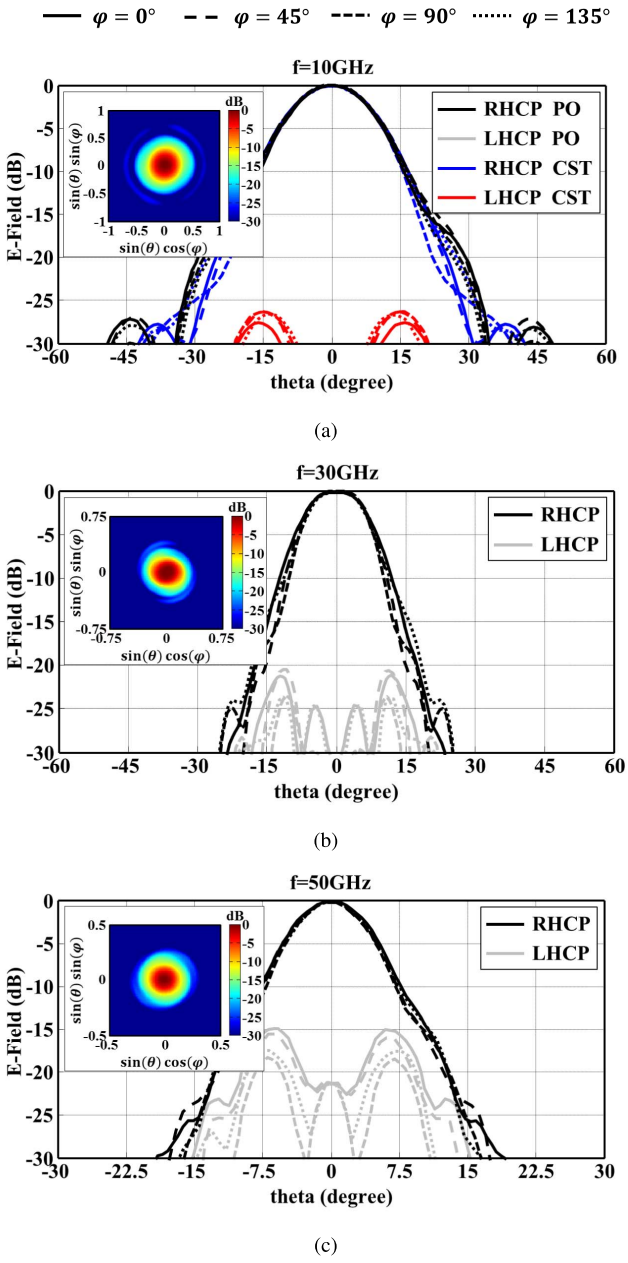

Fig. 18. Simulated radiation patterns outside the lens (secondary fields) illuminated by the enhanced spiral antenna feed at the hyperhemispherical point on different φ planes at the frequencies (a) 10GHz, (b) 30GHz and (c) 50GHz. Insets: 2-D radiation patterns of the RHCP component evaluated with the PO approach.

of the radiation patterns at 10 GHz is shown for the elliptical and the hyperhemispherical extensions, respectively, in Figs. 17(a) and 18(a). A general fair agreement of the radiation patterns has been observed for both cases and for all the frequencies investigated. A discrepancy of the radiation patterns is more relevant only at the lowest frequency because of low accuracy of the PO approximation when the lens is small in terms of the wavelength.

B. Pulse Distortion

The dispersion behavior of the proposed spiral antennas can also be of interest. One of the authors in the past has already shown the absence of dispersion of the radiated pulse by the linear leaky slot antenna in combination with a dense dielectric lens with low extension height [23]. Indeed, lower extension heights lenses lead to lower directivity variation versus frequency. Fig. 19(a) and (b) shows the input pulse and the pulse of the electric field (RHCP component) radiated at broadside in the infinite dielectric and outside the $0.3R$ lens by the regular spiral and the enhanced spiral. In general spiral antennas are known to be dispersive in frequency, due to the fact that the radiation is emitted from different sections of the spiral at different frequencies. There have been authors showing that this dispersion can be reduced by a proper modification of the spiral geometry [21], [22]. A different phenomena drives the dispersion in lenses. For the

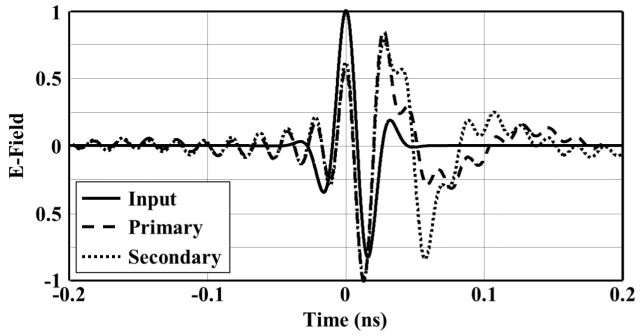

(a)

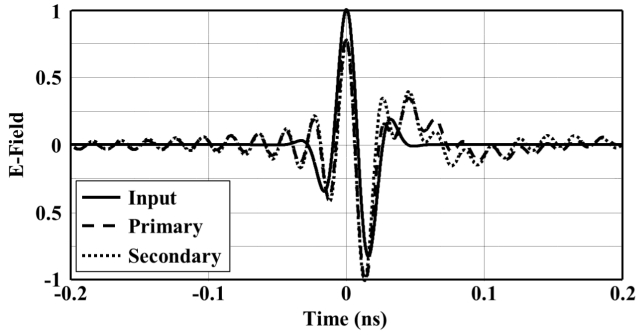

(b)

Fig. 19. Input pulse and primary and secondary simulated electric fields (RHCP component) in time domain at broadside radiated by a dense lens with an extension length $E = 0.3R$, fed by (a) regular spiral and (b) enhanced spiral.

regular spiral case, the pulse radiated inside the dielectric is already significant distorted compared with the input signal. Even more dispersed is the pulse radiated outside the lens. In comparison, the enhanced spiral preserves more the input pulse shape, both for the patterns inside and outside the lens. Indeed the lens does not introduce any additional dispersion. This can be attributed to the fact that the direction of the leaky wave is closer to broadside when an air gap is introduced [23].

VI. Conclusion

In this paper, we have investigated the radiation properties of spiral antennas in the presence of dielectric lenses. We have found that one cannot simply scale the optimal self-complementary geometry typically used for free space. More specifically, the design of a spiral printed between the dielectric and air interface and coupled to a synthesized elliptical lens has been proposed to achieve high aperture efficiency over broad BWs. However, the use of a planar feeding line for this design is only possible if extremely thin substrates are used ($\lambda/2000$) without limiting the BW. Introducing a small air gap between the spiral antenna and the bottom part of the lens allows for decreasing this limitation to $\lambda/200$ and achieving directive patterns without sidelobes for a broadband.

The use of a low extension height hemispherical lens with a spiral kept at small distance from the dielectric is suggested when the main goal of the design is the low frequency dispersivity. A pulse radiated by such antenna presents significantly lower dispersivity than the one radiated by the same lens when fed with a spiral printed directly on the dielectric interface. That is because, the leaky wave radiation associated slots or dipoles printed at the dielectric air interface points toward large angles, while a spiral antenna points toward broadside. Instead when the gap is introduced the leaky wave radiation points at direction closer to broadside. This directivity enhancement achieved inside the dielectric has been validated by measurements of a prototype.

References

[1] D. B. Rutledge and M. S. Muha, "Imaging antenna arrays," *IEEE Trans. Antennas Propag.*, vol. 30, no. 4, pp. 535–540, Jul. 1982.

[2] R. C. Compton, R. McPhedran, Z. Popovic, G. Rebeiz, P. Tong, and D. Rutledge, "Bow-tie antennas on a dielectric half-space: Theory and experiment," *IEEE Trans. Antennas Propag.*, vol. 35, no. 6, pp. 622–631, Jun. 1987.

[3] D. F. Filipovic, S. S. Gearhart, and G. M. Rebeiz, "Double-slot antennas on extended hemispherical and elliptical silicon dielectric lenses," *IEEE Trans. Microw. Theory Techn.*, vol. 41, no. 10, pp. 1738–1748, Oct. 1993.

[4] X. Wu, G. V. Eleftheriades, and T. E. van Deventer-Perkins, "Design and characterization of single- and multiple-beam mm-wave circularly polarized substrate lens antennas for wireless communications," *IEEE Trans. Microw. Theory Techn.*, vol. 49, no. 3, pp. 431–441, Mar. 2001.

[5] E. R. Brown, "THz generation by photomixing in ultrafast photoconductors," *Int. J. High Speed Electron. Syst.*, vol. 13, no. 2, pp. 497–545, 2003.

[6] T. H. Büttengenbach, R. E. Miller, M. J. Wengler, D. M. Watson, and T. G. Phillips, "A broad-band low-noise SIS receiver for submillimeter astronomy," *IEEE Trans. Microw. Theory Techn.*, vol. 36, no. 12, pp. 1720–1726, Dec. 1988.

[7] B. K. Kormanyos, P. H. Ostdiek, W. L. Bishop, T. W. Crowe, and G. M. Rebeiz, "A planar wideband 80–200 GHz subharmonic receiver," *IEEE Trans. Microw. Theory Techn.*, vol. 41, no. 10, pp. 1730–1737, Oct. 1993.

[8] J. M. Edwards, R. O'Brient, A. T. Lee, and G. M. Rebeiz, "Dual-polarized sinuous antennas on extended hemispherical silicon lenses," *IEEE Trans. Antennas Propag.*, vol. 60, no. 9, pp. 4082–4091, Sep. 2012.

[9] A. D. Semenov *et al.*, "Terahertz performance of integrated lens antennas with a hot-electron bolometer," *IEEE Trans. Microw. Theory Techn.*, vol. 55, no. 2, pp. 239–247, Feb. 2007.

[10] M. A. Elmansouri and D. S. Filipovic, "Lens loading approach for improving ultra-wideband performance of spiral antennas," *IET Microw. Antennas Propag.*, vol. 8, no. 12, pp. 937–942, Sep. 2014.

[11] R. Sammeta and D. S. Filipovic, "Improved efficiency lens-loaded cavity-backed transmit sinuous antenna," *IEEE Trans. Antennas Propag.*, vol. 62, no. 12, pp. 6000–6009, Dec. 2014.

[12] V. H. Rumsey, "Frequency independent antennas," in *Proc. IRE Int. Conv. Rec.*, vol. 5. Jul. 1958, pp. 114–118.

[13] Y. Mushiake, "Self-complementary antennas," *IEEE Antennas Propag. Mag.*, vol. 34, no. 6, pp. 23–29, Dec. 1992.

[14] D. B. Rutledge, D. P. Neikirk, and D. P. Kasilingam, "Integrated-Circuit Antennas," *Infrared and Millimeter Waves Part II*, vol. 10. San Diego, CA, USA: Academic Press, 1983.

[15] A. Neto and S. Maci, "Green's function for an infinite slot printed between two homogeneous dielectrics—Part I: Magnetic currents," *IEEE Trans. Antennas Propag.*, vol. 51, no. 7, pp. 1572–1581, Jul. 2003.

[16] S. Maci and A. Neto, "Green's function of an infinite slot printed between two homogeneous dieletrics—Part II: Uniform asymptotic solution," *IEEE Trans. Antennas Propag.*, vol. 52, no. 3, pp. 666–676, Mar. 2004.

[17] J. Dyson, "The equiangular spiral antenna," *IRE Trans. Antennas Propag.*, vol. 7, no. 2, pp. 181–187, Apr. 1959.

[18] J. Dyson, "The unidirectional equiangular spiral antenna," *IRE Trans. Antennas Propag.*, vol. 7, no. 4, pp. 329–334, Oct. 1959.

[19] P. E. Mayes, "Frequency-independent antennas and broad-band derivatives thereof," *Proc. IEEE*, vol. 80, no. 1, pp. 103–112, Jan. 1992.

[20] B. Cheo, V. H. Rumsey, and W. Welch, "A solution to the frequency-independent antenna problem," *IRE Trans. Antennas Propag.*, vol. 9, no. 6, pp. 527–534, Nov. 1961.

[21] M. A. Elmansouri and D. J. Filipovic, "Pulse distortion and mitigation thereof in spiral antenna-based UWB communication systems," *IEEE Trans. Antennas Propag.*, vol. 59, no. 10, pp. 3863–3871, Oct. 2011.

[22] M. A. Elmansouri and D. S. Filipovic, "Low-dispersion spiral antennas," *IEEE Trans. Antennas Propag.*, vol. 60, no. 12, pp. 5522–5530, Dec. 2012.

[23] A. Neto, "UWB, non dispersive radiation from the planarly fed leaky lens antenna—Part 1: Theory and design," *IEEE Trans. Antennas Propag.*, vol. 58, no. 7, pp. 2238–2247, Jul. 2010.
[24] A. Neto, S. Monni, and F. Nennie, "UWB, non dispersive radiation from the planarly fed leaky lens antenna—Part II: Demonstrators and measurements," *IEEE Trans. Antennas Propag.*, vol. 58, no. 7, pp. 2248–2258, Jul. 2010.
[25] D. S. Filipovic and T. Cencich, "Frequency independent antennas," in *Antenna Engineering Handbook*, 4th ed. New York, NY, USA: McGraw-Hill, 2007, ch. 13.
[26] N. Llombart and A. Neto, "THz time-domain sensing: The antenna dispersion problem and a possible solution," *IEEE Trans. THz Sci. Technol.*, vol. 2, no. 4, pp. 416–423, Jul. 2012.
[27] *User Manual, CST Studio Suite*, CST GmbH, Darmstad, Germany, 2012.
[28] A. C. Ludwig, "The definition of cross polarization," *IEEE Trans. Antennas Propag.*, vol. 21, no. 1, pp. 116–119, Jan. 1973.
[29] M. W. Nurnberger and J. L. Volakis, "A new planar feed for slot spiral antennas," *IEEE Trans. Antennas Propag.*, vol. 44, no. 1, pp. 130–131, Jan. 1996.
[30] J. L. Volakis, M. W. Nurnberger, and D. S. Filipovic, "Slot spiral antenna," *IEEE Antennas Propag. Mag.*, vol. 43, no. 6, pp. 15–26, Dec. 2001.
[31] A. Suzuki *et al.*, "Multi-chroic dual-polarization bolometric detectors 560 for studies of the cosmic microwave background," *J. Low Temp. Phys.*, vol. 176, no. 5, pp. 650–656, Sep. 2014, doi: 10.1007/s10909-013-1049-5.
[32] R. O'Brient *et al.*, "A dual-polarized broadband planar antenna and channelizing filter bank for millimeter wavelengths," *Appl. Phys. Lett.*, vol. 102, no. 6, p. 063506, Feb. 2013, doi: 10.1063/1.4791692.
[33] S. J. C. Yates *et al.*, "Photon noise limited radiation detection with lens-antenna coupled microwave kinetic inductance detectors," *Appl. Phys. Lett.*, vol. 99, no. 7, p. 073505, Aug. 2011.
[34] A. Baryshev *et al.*, "Progress in antenna coupled kinetic inductance detectors," *IEEE Trans. THz Sci. Technol.*, vol. 1, no. 1, pp. 112–123, Sep. 2011.
[35] A. Neto, N. Llombart, J. J. A. Baselmans, A. Baryshev, and S. J. C. Yates, "Demonstration of the leaky lens antenna at submillimeter wavelengths," *IEEE Trans. THz Sci. Technol.*, vol. 4, no. 1, pp. 26–32, Jan. 2014.
[36] J. R. Costa, private communication, Jul. 2014.
[37] G. Carluccio and M. Albani, "Efficient adaptive numerical integration algorithms for the evaluation of surface radiation integrals in the high-frequency regime," *Radio Sci.*, vol. 46, no. 5, p. RS0E04, Oct. 2011.
[38] O. Yurduseven, D. Cavallo, A. Neto, G. Carluccio, and M. Albani, "Parametric analysis of extended hemispherical dielectric lenses fed by a broadband connected array of leaky-wave slots," *IET Microw. Antennas Propag.*, vol. 9, no. 7, pp. 611–617, May 2015.
[39] D. Pasqualini and S. Maci, "High-frequency analysis of integrated dielectric lens antennas," *IEEE Trans. Antennas Propag.*, vol. 52, no. 3, pp. 840–847, Mar. 2004.
[40] E. Heyman and L. B. Felsen, "High frequency fields in the presence of a curved dielectric interface," *IEEE Trans. Antennas Propag.*, vol. 32, no. 9, pp. 969–978, Sep. 1984.

Alessandro Garufo (S'13) received the M.Sc. degree in telecommunication engineering from the University of Siena, Siena, Italy, in 2012. He is currently pursuing the Ph.D. degree with the THz Sensing Group, Microelectronics Department, Electrical Engineering, Mathematics, and Computer Science Faculty, Delft University of Technology, Delft, The Netherlands.

He was an Intern with the Antenna Group, Thales Alenia Space, Rome, Italy, from 2011 to 2012, where he developed his master's thesis. He was a Researcher with the Applied Electromagnetic Laboratory, University of Siena, in 2012. His current research interests include analytical and numerical method for antennas and transmission lines characterization, analysis and design of antennas, dielectric lens antennas and antenna arrays with an emphasis on THz frequencies, and THz sources based on photoconductor.

Nuria Llombart (S'06–M'07–SM'13) received the Electrical Engineering and Ph.D. degrees from the Polytechnic University of Valencia, Valencia, Spain, in 2002 and 2006, respectively.

She spent one year with the Friedrich-Alexander University of Erlangen-Nuremberg, Erlangen, Germany, where she was with the Fraunhofer Institute for Integrated Circuits, during her master's studies. Her Ph.D. was pursued with the Antenna Group, TNO Defence, Security and Safety Institute, The Hague, The Netherlands, where she was a Researcher from 2006 to 2007. She was a Post-Doctoral Fellow with the Submillimeter Wave Advance Technology Group, Jet Propulsion Laboratory, California Institute of Technology, Pasadena, CA, USA, from 2007 to 2010. She was a Ramn y Cajal Fellow with the Optics Department, Complutense University of Madrid, Madrid, Spain, from 2010 to 2012. She joined the THz Sensing Group, Microelectronics Department, Electrical Engineering, Mathematics, and Computer Science Faculty, Delft University of Technology, Delft, The Netherlands, in 2012, where she is currently an Associate Professor. She has co-authored over 150 journal and international conference contributions. Her current research interests include the analysis and design of planar antennas, periodic structures, reflector antennas, lens antennas, and waveguide structures, with an emphasis on the THz range.

Dr. Llombart was a co-recipient of the H. A. Wheeler Award for the Best Applications Paper of the Year 2008 in the IEEE TRANSACTIONS ON ANTENNAS AND PROPAGATION, the THz Science and Technology Best Paper Award of the IEEE Microwave Theory and Techniques Society 2014, and several NASA awards. She received the 2014 IEEE Antenna and Propagation Society Lot Shafai Mid-Career Distinguished Achievement Award. In 2015, she also received a European Research Council Starting Grant to perform research on lens antenna arrays for THz coherent cameras. She serves as a Board Member of the IRMMW-THz International Society and an Associate Editor of the *IEEE Antennas and Propagation Wireless Letters*.

Andrea Neto (M'00–SM'10–F'16) received the Laurea degree (*summa cum laude*) in electronic engineering from the University of Florence, Florence, Italy, in 1994, and the Ph.D. degree in electromagnetics from the University of Siena, Siena, Italy, in 2000. Part of his Ph.D. degree was developed with the European Space Agency Research and Technology Center, Noordwijk, The Netherlands.

He was with the Antenna Section, European Space Agency Research and Technology Center, for over two years. He was a Post-Doctoral Researcher with the Submillimeter Wave Advanced Technology Group, California Institute of Technology, Pasadena, CA, USA, from 2000 to 2001. From 2002 to 2010, he was a Senior Antenna Scientist with TNO Defence, Security, and Safety, The Hague, The Netherlands. He was appointed as a Full Professor of Applied Electromagnetism with the Electrical Engineering, Mathematics, and Computer Science Faculty, Delft University of Technology, Delft, The Netherlands, in 2010, where he formed and leads the THz Sensing Group. His current research interests include the analysis and design of antennas, with an emphasis on arrays, dielectric lens antennas, wideband antennas, EBG structures, and THz antennas.

Prof. Neto is a member of the Technical Board of the European School of Antennas and an Organizer of the course on antenna imaging techniques. He is a member of the Steering Committee of the Network of Excellence NEWFOCUS, dedicated to focusing techniques in millimeter and submillimeter wave regimes. In 2011, he received the European Research Council Starting Grant to perform research on advanced antenna architectures for THz sensing systems. He was a co-recipient of the H. A. Wheeler Award for the Best Applications Paper of the Year 2008 in the IEEE TRANSACTIONS ON ANTENNAS AND PROPAGATION, the Best Innovative Paper Prize at the 30th ESA Antenna Workshop in 2008, the Best Antenna Theory Paper Prize at the European Conference on Antennas and Propagation in 2010. He served as an Associate Editor of the IEEE TRANSACTIONS ON ANTENNAS AND PROPAGATION from 2008 to 2013 and the IEEE *Antennas and Wireless Propagation Letters* from 2005 to 2013. He serves as a Topical Editor of the IEEE TRANSACTIONS ON THZ SCIENCE AND TECHNOLOGY.